THE JOURNAL OF PHYSICAL CHEMISTRY C

ARTICLE

pubs.acs.org/JPCC

DFT-Based Study on Oxygen Adsorption on Defective Graphene-Supported Pt Nanoparticles

Dong-Hee Lim and Jennifer Wilcox*

Department of Energy Resources Engineering, Stanford University, 367 Panama Street, Green Earth Sciences, Stanford, California 94305-2220

Supporting Information

ABSTRACT: The structural and electronic properties of Pt_{13} nanoparticles adsorbed on monovacancy defective graphene have been determined to understand oxygen adsorption on Pt nanoparticles based upon density functional theory predictions using the generalized gradient approximation. We demonstrate that a monovacancy site of graphene serves a key role as an anchoring point for Pt_{13} nanoparticles, ensuring their stability on defective graphene surfaces and suggesting their enhanced catalytic activity toward the interaction with O_2. Strong hybridization of the Pt_{13} nanoparticle with the sp^2 dangling bonds of neighboring carbon atoms near the monovacancy site leads to the strong binding of the Pt_{13} nanoparticle on defective graphene (−7.45 eV in adsorption energy). Upon both adsorption of the Pt_{13} nanoparticle on defective graphene and O_2 on Pt_{13}−defective graphene, strong charge depletion of the Pt atom at the interfaces of Pt−C and Pt−O_2 is observed. Pt_{13} nanoparticles are able to donate charge to both defective graphene and O_2. The Pt_{13}−defective graphene complex shows an O_2 adsorption energy of −2.30 eV, which is weaker than the O_2 adsorption energy of −3.92 eV on a free Pt_{13} nanoparticle. Considering the strong stability of the Pt nanoparticles and relatively weaker O_2 adsorption energy due to the defective graphene support, we expect that the defective graphene support may increase the catalytic activity of Pt nanoparticles compared to flat Pt metal surfaces, not only by preventing sintering of Pt nanoparticles due to the strong anchoring nature of the graphene defect sites but also by providing a balance in the O_2 binding strength that may allow for enhanced catalyst turnover.

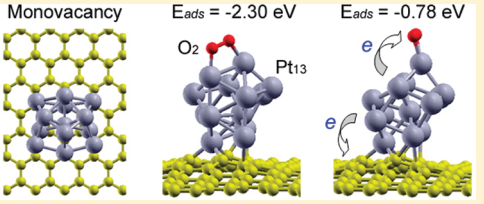

1. INTRODUCTION

Graphene, one planar sheet of sp^2-bonded carbon atoms arranged in a hexagonal lattice, has recently attracted wide attention in materials science and condensed-matter physics due to its unique electronic properties.[1−3] The presence of carbon vacancies on graphene significantly influences the physical and chemical characteristics and magnetic properties of graphene.[4−6] Carbon vacancies induce magnetism by breaking the symmetry of nonmagnetic perfect graphene.[6−9] The vacancy sites in graphene can be used as anchoring points for the growth of nanoparticles. The binding of Fe and Al nanoparticles, for example, is significantly enhanced due to sp^2 dangling carbon bonds at a monovacancy site of defective graphene.[5] These defective graphene-supported nanoparticles may enhance surface reactivity.[5,10] Previous experimental studies have shown that atomic defects in graphene sheets can be formed after several tens of seconds of irradiation with an electron beam[11] or by treatment with hydrochloric acid.[12]

Platinum (Pt) nanoparticles are considered in the current study with specific focus on the changes of mechanical and electronic properties from the bulk phase to the nanoparticle-scale, with interest to the oxygen reduction reaction (ORR). Platinum has been represented as one of the best electrocatalysts for ORR with most of the previous Pt ORR studies focusing on different types of Pt surface models (i.e., Pt(111), Pt(110), or Pt(100))[13−15] or cluster models.[16,17] The ORR has been of central focus amidst the ongoing studies of electrode reactions in low-temperature fuel cells. The slow kinetics of this reaction is limiting its application, although efforts are being pursued to try and advance its performance to achieve improved efficiency.[14,18−20]

Recently, composites of graphene with deposited metal nanoparticles (e.g., Pt, Au, and Pd) have been proposed as effective nanocomposites for fuel cell applications,[21−23] with the graphene−metal nanocomposites casted as films on electrode surfaces.[21,22] Pt nanoparticles supported on functionalized graphene sheets have showed enhanced activity and stability of Pt catalysts for electrocatalytic oxygen reduction in proton-exchange membrane (PEM) fuel cells.[22] The enhanced activity of Pt nanoparticles on functionalized graphene may be attributed to enhancement of the electrochemically active surface area.[21]

Experimental work carried out by Sakurai et al.[24] indicate that transition-metal clusters (Fe, Ti, Zr, Nb, and Ta) with "magic numbers" n,[24,25] such that, n = 7, 13, and 15 atoms in a given cluster, have a higher geometric and/or electronic stability than other cluster sizes. For the current study, n = 13 has been chosen to investigate the interaction of a Pt nanoparticle on defective graphene and the adsorption of oxygen on the defective-graphene-supported Pt nanoparticle.

Received: June 3, 2011
Revised: October 11, 2011
Published: October 11, 2011

For ORR investigations, the essential first step is to elucidate the behavior of oxygen adsorption on Pt nanoparticles. The purpose of the current study is to utilize defective graphene-supported Pt nanoparticles for the enhancement of the catalytic activity of Pt nanoparticles toward oxygen reduction. For this, the current study investigates the following two adsorption studies: (1) Pt_{13} nanoparticle adsorption on a monovacancy defect site of graphene and (2) oxygen adsorption on the Pt_{13}−defective graphene. The current study also provides details of the structural and electronic properties of these investigated systems.

2. COMPUTATIONAL METHODOLOGY

Spin-polarized density functional theory calculations were performed using the Vienna *ab initio* Simulation Package (VASP)[26−29] with the projector-augmented wave (PAW)[30,31] method to calculate the electronic and atomic structures and energies of Pt nanoparticle-graphene systems. Electron exchange-correlation functionals were represented with the generalized gradient approximation (GGA), and the model of Perdew, Burke and Ernzerhof (PBE)[32] was used for the nonlocal corrections. An orthorhombic supercell of 19.74 × 17.10 × 32.01 Å with periodic boundary conditions was used for the nanoparticle−graphene systems. The nanoparticle−graphene system was separated from its periodic images in the z direction by a vacuum space of 25.5 Å. A dipole moment correction was not incorporated due to its negligible effect on adsorption energy of Fe_{13} nanoparticles on a monovacancy defective graphene.[5] A kinetic energy cutoff of 400 eV was used with a plane-wave basis set. The integration of the Brillouin zone was conducted using a 2 × 2 × 1 Monkhorst−Pack grid[33] with the Γ-point included and first-order Methfessel−Paxton smearing[34] with a width of 0.1 eV. All atoms were fully relaxed and optimized until the forces were reduced below 0.02 eV/Å.

The supercell used for a monovacancy defective graphene consists of 127 carbon atoms with a single carbon atom vacancy at the center. The isolated Pt_{13} nanoparticle was optimized in a 30.0 Å cubic supercell in which the Brillouin zone integration was carried out for the Γ-point only. For O_2 in the gas phase, the calculations predict an oxygen bond length of 1.23 Å and bond dissociation energy of 6.07 eV. Both are larger than experimental data (i.e., bond length of 1.21 Å and bond dissociation energy of 5.17 eV).[35] Other DFT studies predict O_2 bond lengths of 1.24[36] and 1.22[37] Å and bond dissociation energies of 5.73[37] and 6.24[32] eV, which are comparable with the predictions of the current work. The adsorption energy (E_{ads}) of a Pt_{13} nanoparticle (or O_2) per adsorbate is calculated as

$$E_{ads} = \frac{1}{N_{adsorbate}}\left(E_{substrate+adsorbate} - E_{substrate} - N_{adsorbate}E_{adsorbate}\right) \quad (1)$$

where $N_{adsorbate}$ is the number of an adsorbate in the model system. $E_{substrate+adsorbate}$, $E_{substrate}$, and $E_{adsorbate}$ are the total energies of Pt_{13}−defective graphene (or O_2−Pt_{13}−defective graphene), defective graphene (or Pt_{13}−defective graphene), and gas phase Pt nanoparticle (or O_2). A negative adsorption energy indicates that adsorption is exothermic (stable) with respect to the free nanoparticle cluster.

For the charge difference density ($\Delta n(\mathbf{r})$) plot of the O_2−Pt_{13}−defective graphene system upon O_2 adsorption, the charge densities of the system ($n(\mathbf{r})_{system}$) and its separated constitutes of the O_2 adsorbate ($n(\mathbf{r})_{adsorbate}$) and Pt_{13}−defective graphene substrate ($n(\mathbf{r})_{substrate}$) were integrated in x and y directions (parallel to the surface), and $\Delta n(\mathbf{r})$ was calculated as $n(\mathbf{r})_{system} - [n(\mathbf{r})_{adsorbate} + n(\mathbf{r})_{substrate}]$. The source of the isolated O_2 and Pt_{13}−defective graphene structures has been directly obtained from the optimized structure of the O_2 adsorbed Pt_{13}−defective graphene system and then reoptimized by relaxing x and y directions while freezing the z directions. The Bader charge analysis[38−40] has been carried out by using the optimized geometries of free O_2, Pt_{13}−defective graphene, and O_2 adsorbed Pt_{13}−defective graphene with a second finer fast Fourier transform (FFT)-mesh 4 times that used in the adsorption calculations.

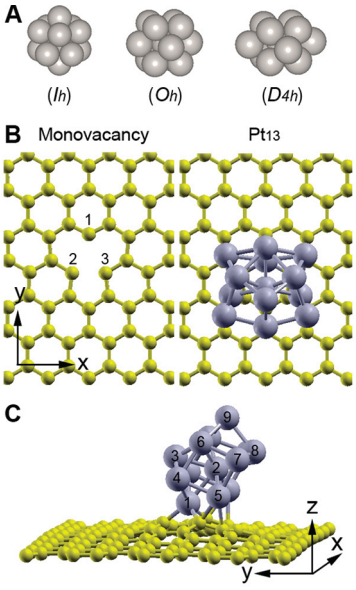

Figure 1. (A) Pt_{13} nanoparticles. (B) Top view and (C) side view of the adsorbed Pt_{13} nanoparticle on the monovacancy site of graphene. Yellow and gray colors represent C and Pt, respectively.

3. RESULTS AND DISCUSSION

Interaction of Pt_{13} Nanoparticle on Defective Graphene. Prior to the investigation of Pt_{13} nanoparticle adsorption on defective graphene, a stable configuration of isolated Pt_{13} nanoparticle was sought by optimizing three different geometries of Pt_{13} nanoparticles in the gas phase: icosahedron (I_h), regular cuboctahedron (O_h), and distorted cuboctahedron (D_{4h}) as shown in Figure 1A. The distorted cuboctahedron (D_{4h}) configuration is more stable than the other symmetry configurations showing ∼1 eV lower total energy. This result is consistent with a previous DFT study of Pt nanoclusters showing that the lowest energy configuration of Pt_{13} is a symmetry-broken D_{4h} rather than icosahedral configuration.[41] The cluster radii of the Pt_{13} D_{4h} configuration are 2.49 and 3.13 Å for the nearest and next nearest Pt atoms from the center Pt atom, respectively. Bare defective graphene with a monovacancy site has a magnetic moment of 1.20 μ_B, whereas perfect graphene is nonmagnetic. The magnetic moment is attributed to the C1 unsaturated bond rather than the C2 and C3 atoms that form a weak bonding interaction (i.e., 2.03 Å, shorter than 2.47 Å of perfect graphene) in Figure 1B.[5] Details of spin density analysis supporting the localized magnetic moment of C1 at the carbon vacancy site of bare defective graphene are available in the Supporting Information, Figure S1.

For Pt_{13} nanoparticle adsorption on defective graphene, the current study tested three different adsorption configurations of Pt_{13} D_{4h} based on the adsorption studies of Fe_{13} and Al_{13} nanoparticles on monovacancy defective graphene,[5] in which one nanoparticle edge atom interacts with three sp^2 dangling bonds of carbon at the monovacancy site showing exceptional stability compared to the other modes where two or three nanoparticle atoms are placed near the monovacancy site. Figure 1 panels B and C, represent the most stable adsorption configurations of the Pt_{13} nanoparticle on the monovacancy site of graphene. The adsorption energy for the most stable Pt_{13} D_{4h} nanoparticle is found to be −7.45 eV. The strong interaction between the nanoparticle and the carbon-vacancy defect in graphene is attributed to the sp^2 dangling bond formed at the three neighboring carbon atoms near the vacancy[5,42] due to the carbon−carbon bond cleavage.[6−8] The full geometries of the other adsorption configurations are available in Supporting Information, Figure S2.

Upon adsorption, both geometries of the adsorbed Pt_{13} nanoparticles and the initially planar surface of defective graphene are distorted and strongly reconstructed. The initially planar surface of defective graphene strongly reconstructs with relaxation normal to the surface (i.e., in the z direction), especially near the defect site while lateral relaxation of the graphene lattice is not significant as shown in Figure 1C. The height of the carbon atoms near the defect site increases up to 1.33 Å, which is similar with the elevated heights of carbon atoms shown in the Fe_{13} (1.09 Å) and Al_{13} (1.48 Å) nanoparticle adsorption on the monovacancy site of defective graphene.[5] The elevated heights of carbon atoms at the monovacancy site are ordered as Fe < Pt < Al nanoparticle systems. This may be attributed to the atomic radii of Fe (1.26 Å) < Pt (1.39 Å) < Al (1.43 Å).[5]

The projected density of states (PDOS) has been analyzed for the valence electrons of the isolated Pt_{13} nanoparticle and defective graphene in addition to the adsorbed complexes. The PDOS analyses are useful for understanding the details of the interaction between the Pt_{13} nanoparticle and defective graphene. Figure 2 shows plots of the PDOS of the s, p, and d states of bound Pt (Pt1 in Figure 1C) and the s and p states of carbon nearest from monovacancy site of graphene. Pt atoms in the isolated Pt_{13} nanoparticle show narrow and sharp bands characterized by a set of discrete levels in a finite system[43] (data not shown here). However, Pt atoms in the adsorbed nanoparticle represent delocalized, broadened, and strongly modified bands ranging from −15 to +7 eV in Figure 2A, which is similar to the PDOS of the Pt(111)[44] metal surface. Comparing the PDOS of Pt and C atoms in Figure 2, strong hybridization between Pt 5d states and C 2p states of defective graphene occurs through almost the entire energy region, supporting a covalent bonding interaction between Pt and C atoms as described in a Pt^+−C example.[45] These broadened and strongly modified states of Pt indicate a strong hybridization of the Pt nanoparticle with the sp^2 dangling bonds of carbon at the monovacancy site of graphene.

Figure 3 displays excess Bader charges of the Pt_{13}−defective graphene system indicating relatively strong charge accumulation at the neighboring carbon atoms near the monovacancy due to the interaction between the sp^2 dangling bonds of the carbon atoms and the Pt nanoparticle. Also, relatively strong charge depletion is found near the bound Pt atom (Pt1 in both Figures 1C and 3). Bader charge analysis reveals negative excess charges on the bound Pt atom of −0.41e and positive excess

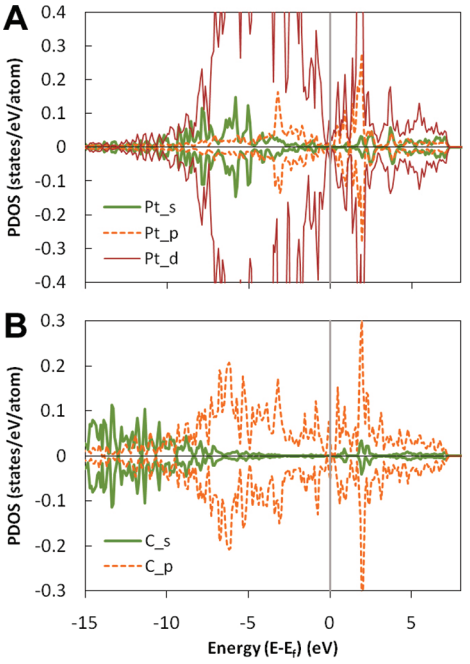

Figure 2. (A) PDOS of s, p, and d states of bound Pt (Pt1 in Figure 1C) at the monovacancy site of graphene. (B) PDOS of s and p states of carbon nearest from the monovacancy after adsorption. Spin-up (↑) and spin-down (↓) states are marked as positive and negative values, respectively. The Fermi energy is referenced at 0 eV.

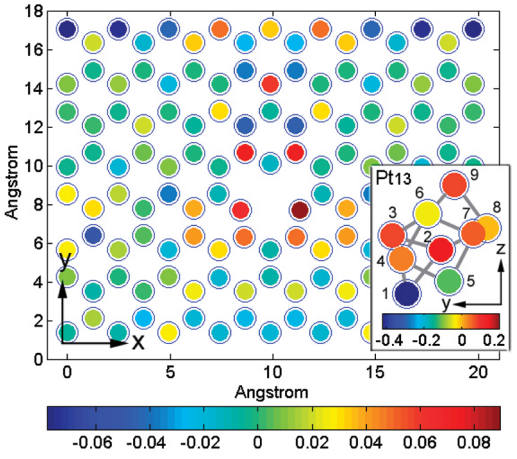

Figure 3. Excess Bader charges (in units of e) of the monovacancy defective graphene and adsorbed Pt_{13} (in the inset) in the Pt_{13}−defective graphene system. Numbers 1−9 in the inset represent Pt atoms as depicted in Figure 1C.

charges (up to 0.05−0.09e) on carbon atoms neighboring the monovacancy site. Total net excess charge on the defective graphene is 0.24e. This indicates that charges are transferred from bound Pt to defective graphene, in particular to the sp^2 dangling bonds of carbon atoms near the vacancy site. Lim et al.[5] conducted Fe_{13} and Al_{13} nanoparticle adsorption on the monovacancy defective graphene and reported that excess charges on bound Fe and Al atoms at the monovacancy site were −0.47 and −1.72e, respectively, and total net excess charges on the defective graphene were 1.57 and 3.08e for the Fe_{13} and Al_{13} nanoparticle

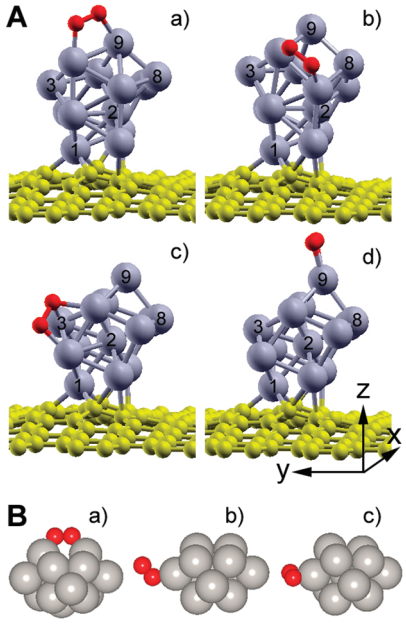

Figure 4. (A) O_2 adsorption on defective graphene-supported Pt_{13} nanoparticles: O_2 adsorption energies of (a) −2.30, (b) −1.96, (c) −1.80, and (d) −0.78 eV. (B) O_2 adsorption on free Pt_{13} nanoparticles optimized in the gas phase: O_2 adsorption energies of (a) −3.92 in a bridge, (b) −1.20 in a vertical (Pauling model), and (c) −1.19 eV in an atop (Griffit model) mode. Red, yellow, and gray colors represent O, C, and Pt, respectively.

systems, respectively. The amount of charge transferred from the Pt, Fe, and Al nanoparticles to defective graphene is ordered as, Pt (0.24*e*) < Fe (1.57*e*) < Al (3.08*e*). This can be explained by the difference in both the work functions of Pt (5.64 eV),[35] Fe (4.67 eV),[35] and Al (4.06 eV)[35] and the ionization potentials of Pt (8.96 eV),[46] Fe (7.90 eV),[46] and Al (5.99 eV).[46] The work function (Φ) and ionization potential (IP) are important electronic properties for evaluating the charge transfer between adsorbate and substrate since both terms refer to the energy required to remove electrons from an adsorbate−substrate system. Although the work function is not always governed by the quantity of adsorbate-induced charge transfer,[47] charges are generally more likely transferred to substrates from adsorbates with lower Φ and IP.

Interaction of O_2 on Pt_{13}−Defective Graphene. To determine the possible O_2 adsorption configurations on the defective graphene-supported Pt_{13} nanoparticle, a simple Pt_{13} model was used for preliminary tests to offer insight into O_2 adsorption on the supported Pt_{13} nanoparticle. The simple Pt_{13} model was directly obtained from the adsorbed Pt_{13} nanoparticle configuration shown in Figure 1C by removing defective graphene and freezing only Pt1 (bound Pt) to mimic the anchored Pt atom at the monovacancy site of graphene. After examining the relative total energies of 16 different O_2 adsorption configurations on the simple Pt_{13} model including bridge, vertical (Pauling model), and atop (Griffit model) modes,[48,49] it has been found that O_2 prefers to bind on the simple Pt_{13} model in a bridge configuration as shown in the Supporting Information, Table S1. Among the 16 possible initial O_2 adsorption configurations on the simple Pt_{13} model, three bridge configurations and one atop configuration were fully reoptimized on the monovacancy site of defective graphene. As shown in Figure 4A, stable O_2 adsorption configurations on the defective graphene-supported Pt_{13} nanoparticles have adsorption energies of −2.30 eV in the bridge configuration (a) and −0.78 eV in the atop configuration (d). The predicted O_2 adsorption energy in the bridge configuration is significantly enhanced compared to other studies of O_2 adsorption, which range among −0.58 to −0.72 eV on Pt(111),[50] −1.30 eV on Pt(001),[51] −1.48 eV on Pt(110),[52] −1.42 eV on a Pt_2 cluster,[53] −1.08 eV on a Pt_3 cluster,[53] and −0.53 to −0.83 eV on Pt_n clusters (n = 2−5).[54] The O_2 bond length of 1.23 Å as a free gas-phase molecule is more elongated upon adsorption on defective graphene-supported Pt_{13} systems, i.e., as 1.44 and 1.38 Å for the bridge and atop configurations, respectively, compared to 1.35 Å[36] on Pt(111). A strong linear relationship is observed between elongated O_2 bond lengths and transferred charge amounts to O_2 (R^2 = 0.98); the more charge transferred to O_2 from the Pt_{13}−defective graphene system, the more elongated the O−O bonds become. Table S2 in the Supporting Information summarizes the elongated O_2 bond lengths and the excess Bader charge of the components of the Pt_{13}−defective graphene systems (this Bader charge analyses were conducted with the same FFT-mesh as used in the adsorption calculations to save computational effort).

Although defective graphene-supported Pt_{13} nanoparticles may enhance O_2 adsorption, the adsorption energies are higher (less stable) than those of the free Pt_{13} nanoparticles optimized in the gas phase. Figure 4B shows O_2 adsorption on free Pt_{13} nanoparticles, exhibiting a greater exothermic O_2 adsorption energy of up to −3.92 eV in the bridge configuration compared to that of defective graphene-supported Pt_{13} nanoparticles. This exceptionally stable O_2 adsorption brings significant distortion to the free Pt_{13} nanoparticle compared to other O_2−free Pt_{13} systems as shown in Figure 4B (more configurations of O_2−free Pt_{13} systems in Supporting Information, Figure S3). Traditionally, stronger adsorption leads to a greater distortion in adsorbate−substrate systems as discussed in the previous work,[5] concerning Fe_{13} and Al_{13} nanoparticle adsorption on defective graphene. In other words, an adsorbate−substrate system that provides more degrees of freedom for geometry distortion may be better suited for allowing enhanced adsorption between an adsorbate and substrate. To test this hypothesis, O_2 adsorption energies on the free Pt_{13} nanoparticle were recalculated by freezing the positions of the atoms in the Pt_{13} nanoparticle. Two adsorption sites were examined, i.e, the most and least stable sites as illustrated in Figure 4B (a) and (c), with adsorption energies of −1.14 and −1.07 eV, respectively. Compared to the fully relaxed Pt_{13} nanoparticles (−3.92 and −1.19 eV for the most and least stable sites, respectively), this result indicates that the significant enhancement of the oxygen interaction with free Pt_{13} nanoparticles is attributed to the geometry distortion of the free Pt_{13} nanoparticle upon O_2 adsorption. Additional views of Figure 4B (a) are shown in the Supporting Information, Figure S4, that further illustrate the extent of distortion upon O_2 adsorption.

The monovacancy defective graphene support stably anchors a Pt_{13} nanoparticle at the vacancy site and consequently prevents the Pt_{13} nanoparticle from being significantly altered upon O_2 adsorption. This may explain the weaker O_2 adsorption energies on the defective graphene-supported Pt_{13} system compared to those of the free Pt_{13} nanoparticle, which may furthermore be beneficial to this system's potential catalytic applications, e.g, oxygen reduction reaction. For instance, if a reactant binds too strongly to a catalyst surface, it can substantially decrease the turnover frequency. Rather, a balance in the binding strength should be sought. It should be duly noted that larger Pt nanoparticles

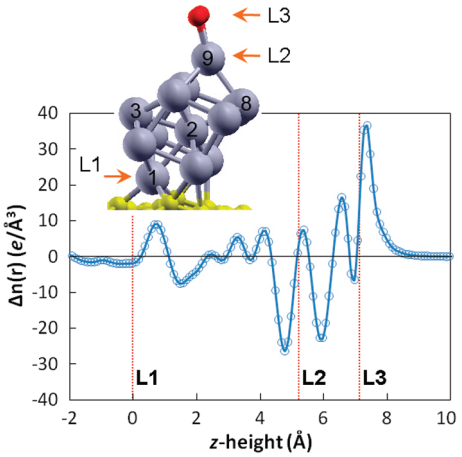

Figure 5. Charge difference density of integrated charge densities in the x and y directions normal to the surface for adsorbed O_2 on the monovacancy defective graphene-supported Pt_{13} nanoparticle. L1, L2, and L3 represent the bottom and top Pt layers and O_2 layer, respectively. The L1 layer is referenced at 0 Å in z height. Red, gray, and yellow colors represent O, Pt, and C, respectively.

(>Pt_{13}) that provide less degrees of freedom for geometry distortion upon O_2 adsorption might behave differently in terms of O_2 adsorption strength between defective graphene-supported and free Pt systems.

Figure 5 displays the charge difference density, $\Delta n(\mathbf{r})$, of integrated charge densities in x and y directions (parallel to the surface), which are plotted with respect to the z direction. As discussed in previous work,[5] the charge difference density may be underestimated or overestimated when an adsorbate is significantly distorted upon adsorption. The magnitude of charge depletion of an Al nanoparticle upon adsorption on defective graphene was, for example, underestimated due to significant geometry expansion of the Al nanoparticle.[5] Thus, the least-modified adsorption geometry of the O_2−Pt_{13}−graphene system [Figure 4A(d)] was chosen for the charge difference density analysis. As seen in Figure 5 (z height between L2 and L3), appreciable charge depletion from the vicinity of the top Pt atom (Pt9) and charge accumulation in the vicinity of O_2 is observed, indicating qualitatively that charges are transferred from Pt to O_2 at the Pt−O_2 interface. This electron transfer from Pt to O_2 is also reported by another DFT study regarding O_2 adsorption on Pt(111).[55] The overall electron transfer scheme may include electron donation from the O_2 2π orbital to the Pt $5d_{z^2}$ orbital and simultaneous back-donation from the partially filled Pt $5d_{xz}$ or $5d_{yz}$ orbital to the O_2 $2\pi^*$ orbital as proposed by Toda et al.[56,57] The $\Delta n(\mathbf{r})$ of the inner Pt_{13} nanoparticle (z height from L1 to L2 in Figure 5) is more likely to be of the Friedel oscillation type (i.e, persistent oscillations of the electronic state density due to boundary effects[58]) rather than a net transfer, which is very similar behavior to that of the O_2 adsorbed−Pt(111) bulk layers.[55]

4. CONCLUSION

The current study demonstrates two potential benefits of the use of defective graphene as a support for the catalytic activity of Pt nanoparticles, i.e., enhanced stability of surface-bound Pt nanoparticles and possible tunability of the O_2 adsorption strength. The monovacancy site of graphene plays a key role in anchoring the Pt_{13} nanoparticles, yielding a relatively strong adsorption energy of −7.45 eV due to the strong hybridization of the Pt nanoparticle with the sp^2 dangling bonds of neighboring carbon atoms near the monovacancy site of graphene. This enhanced stability may provide minimal Pt nanoparticle aggregation on the graphene surface.

Upon adsorption of a Pt_{13} nanoparticle on the monovacancy defect site of graphene, charge is transferred mostly from the bound Pt atom at the monovacancy site to defective graphene, accumulating a total net charge of 0.24e on defective graphene. The O_2 adsorption on the defective graphene-supported Pt_{13} nanoparticle leads to a charge depletion of Pt, while O_2 accumulates charge at the Pt−O_2 interface. O_2 adsorption energies on the Pt_{13}−defective graphene complex and the free Pt_{13} nanoparticle are −2.30 and −3.92 eV, respectively. This weakened O_2 adsorption energy due to the defective graphene support may contribute to the potential optimization of the catalytic activity of Pt nanoparticles toward oxygen reduction by providing a balance in the O_2 binding strength thereby allowing for an optimal turnover .

■ ASSOCIATED CONTENT

Supporting Information. Spin density and geometry at the carbon vacancy site of bare defective graphene, two other less stable adsorption configurations of Pt_{13} nanoparticles on the monovacancy defective graphene, relative total energies of O_2−Pt_{13} simple models, elongated O_2 bond lengths and excess Bader charge of the O_2−Pt_{13}−defective graphene systems, and O_2 adsorption on free Pt_{13} nanoparticles. This material is available free of charge via the Internet at http://pubs.acs.org.

■ AUTHOR INFORMATION

Corresponding Author

*E-mail: wilcoxj@stanford.edu. Phone: (650) 724-9449. Fax: (650) 725-2099.

■ ACKNOWLEDGMENT

This material is based upon work supported as part of the Center on Nanostructuring for Efficient Energy Conversion (CNEEC) at Stanford University, an Energy Frontier Research Center funded by the U.S. Department of Energy, Office of Science, Office of Basic Energy Sciences under Award Number DE-SC0001060. The computational resources were supported by the National Science Foundation through TeraGrid resources provided by TACC.

■ REFERENCES

(1) Katsnelson, M. I. *Mater. Today* **2007**, *10*, 20.
(2) Geim, A. K.; Novoselov, K. S. *Nat. Mater.* **2007**, *6*, 183.
(3) Neto, A. H. C.; Guinea, F.; Peres, N. M. R.; Novoselov, K. S.; Geim, A. K. *Rev. Mod. Phys.* **2009**, *81*, 109.
(4) Carlsson, J. M.; Scheffler, M. *Phys. Rev. Lett.* **2006**, *96*, 046806.
(5) Lim, D.-H.; Negreira, A. S.; Wilcox, J. *J. Phys. Chem. C* **2011**, *115*, 8961.
(6) Ma, Y.; Lehtinen, P. O.; Foster, A. S.; Nieminen, R. M. *New J. Phys.* **2004**, *6*, 68.
(7) Yazyev, O. V.; Helm, L. *Phys. Rev. B* **2007**, *75*, 125408.
(8) Singh, R.; Kroll, P. *J. Phys.: Condens. Matter* **2009**, *21*, 196002.
(9) Nelayev, V. V.; Mironchik, A. I. *Mater. Phys. Mech.* **2010**, *9*, 26.
(10) Simon, P.; Gegotsi, Y. *Nat. Mater.* **2008**, *7*, 845.

(11) Hashimoto, A.; Suenaga, K.; Gloter, A.; Urita, K.; Iijima, S. *Nature* **2004**, *430*, 870.
(12) Coleman, V. A.; Knut, R.; Karis, O.; Grennberg, H.; Jansson, U.; Quinlan, R.; Holloway, B. C.; Sanyal, B.; Eriksson, O. *J. Phys. D: Appl. Phys.* **2008**, *41*, 062001.
(13) Marković, N. M.; Schmidt, T. J.; Stamenković, V.; Ross, P. N. *Fuel Cells* **2001**, *1*, 105.
(14) Wang, Y. X.; Balbuena, P. B. *J. Phys. Chem. B* **2005**, *109*, 14896.
(15) Lamas, E. J.; Balbuena, P. B. *J. Chem. Theory Comput.* **2006**, *2*, 1388.
(16) Sidik, R. A.; Anderson, A. B. *J. Electroanal. Chem.* **2002**, *528*, 69.
(17) Tsuda, M.; Kasai, H. *J. Phys. Soc. Jpn.* **2007**, *76*, 024801.
(18) Yeager, E. *Electrochim. Acta* **1984**, *29*, 1527.
(19) Nørskov, J. K.; Rossmeisl, J.; Logadottir, A.; Lindqvist, L.; Kitchin, J. R.; Bligaard, T.; Jónsson, H. *J. Phys. Chem. B* **2004**, *108*, 17886.
(20) Calvo, S. R.; Balbuena, P. B. *Surf. Sci.* **2007**, *601*, 165.
(21) Seger, B.; Kamat, P. V. *J. Phys. Chem. C* **2009**, *113*, 7990.
(22) Kou, R.; Shao, Y.; Wang, D.; Engelhard, M. H.; Kwak, J. H.; Wang, J.; Viswanathan, V. V.; Wang, C.; Lin, Y.; Wang, Y.; Aksay, I. A.; Liu, J. *Electrochem. Commun.* **2009**, *11*, 954.
(23) Xu, C.; Wang, X.; Zhu, J. *J. Phys. Chem. C* **2008**, *112*, 19841.
(24) Sakurai, M.; Watanabe, K.; Sumiyama, K.; Suzuki, K. *J. Chem. Phys.* **1999**, *111*, 235.
(25) Lian, L.; Su, C. X.; Armentrout, P. B. *J. Chem. Phys.* **1992**, *97*, 4072.
(26) Kresse, G.; Hafner, J. *Phys. Rev. B* **1993**, *47*, 558.
(27) Kresse, G.; Hafner, J. *Phys. Rev. B* **1994**, *49*, 14251.
(28) Kresse, G.; Furthmüller, J. *Phys. Rev. B* **1996**, *54*, 11169.
(29) Kresse, G.; Furthmüller, J. *Comput. Mater. Sci.* **1996**, *6*, 15.
(30) Blöchl, P. E. *Phys. Rev. B* **1994**, *50*, 17953.
(31) Kresse, G.; Joubert, D. *Phys. Rev. B* **1999**, *59*, 1758.
(32) Perdew, J. P.; Burke, K.; Ernzerhof, M. *Phys. Rev. Lett.* **1996**, *77*, 3865.
(33) Monkhorst, H. J.; Pack, J. D. *Phys. Rev. B* **1976**, *13*, 5188.
(34) Methfessel, M.; Paxton, A. T. *Phys. Rev. B* **1989**, *40*, 3616.
(35) 5*CRC Handbook of Chemistry and Physics*, Haynes, W. M., 91st ed. (Internet Version); CRC Press/Taylor and Francis: Boca Raton, FL, 2011.
(36) Tripković, V.; Skúlason, E.; Siahrostami, S.; Nørskov, J. K.; Rossmeisl, J. *Electrochim. Acta* **2010**, *55*, 7975.
(37) Ge, Q.; Hu, P.; King, D. A.; Lee, M. H.; White, J. A.; Payne, M. C. *J. Chem. Phys.* **1997**, *106*, 1210.
(38) Bader, R. F. W. *Chem. Rev.* **1991**, *91*, 893.
(39) Henkelman Group; The University of Texas at Austin, http://theory.cm.utexas.edu/henkelman/research/bader/.
(40) Tang, W.; Sanville, E.; Henkelman, G. *J. Phys.: Condens. Matter* **2009**, *21*, 084204.
(41) Apra, E.; Fortunelli, A. *J. Phys. Chem. A* **2003**, *107*, 2934.
(42) Zhou, M.; Zhang, A. H.; Dai, Z. X.; Zhang, C.; Feng, Y. P. *J. Chem. Phys.* **2010**, *132*, 194704.
(43) Cuong, N. T.; Fujiwara, A.; Mitani, T.; Chi, D. H. *Comput. Mater. Sci.* **2008**, *44*, 163.
(44) Hammer, B.; Morikawa, Y.; Norskov, J. K. *Phys. Rev. Lett.* **1996**, *76*, 2141.
(45) Armentrout, P. B. *Int. J. Mass Spectrom.* **2003**, *227*, 289.
(46) Drake, G. W. F. *Springer Handbooks of Atomic, Molecular, and Optical Physics*; Springer: Würzburg, Germany, 2006.
(47) Leung, T. C.; Kao, C. L.; Su, W. S.; Feng, Y. J.; Chan, C. T. *Phys. Rev. B* **2003**, *68*, 195408.
(48) Yeager, E. *J. Electrochem. Soc.* **1981**, *128*, 160C.
(49) Adžić, R. R.; Wang, J. X. *J. Phys. Chem. B* **1998**, *102*, 8988.
(50) Zhang, J. *PEM Fuel Cell Electrocatalysts and Catalyst Layers-Fundamentals and Applications*, Zhang, J., Ed.; Springer-Verlag London Ltd.: London, 2008.
(51) Escaño, M. C. S.; Nakanishi, H.; Kasai, H. *J. Phys. Soc. Jpn.* **2009**, *78*, 064603.
(52) Petersen, M. A.; Jenkins, S. J.; King, D. A. *J. Phys. Chem. B* **2006**, *110*, 11962.
(53) Balbuena, P. B.; Altomare, D.; Agapito, L.; Seminario, J. M. *J. Phys. Chem. B* **2003**, *107*, 13671.
(54) Li, T.; Balbuena, P. B. *J. Phys. Chem. B* **2001**, *105*, 9943.
(55) Qi, L.; Qian, X. F.; Li, J. *Phys. Rev. Lett.* **2008**, *101*, 146101.
(56) Toda, T.; Igarashi, H.; Uchida, H.; Watanabe, M. *J. Electrochem. Soc.* **1999**, *146*, 3750.
(57) Lai, F. J.; Chou, H. L.; Sarma, L. S.; Wang, D. Y.; Lin, Y. C.; Lee, J. F.; Hwang, B. J.; Chen, C. C. *Nanoscale* **2010**, *2*, 573.
(58) Friedel, J. *Nuovo Cimento* **1958**, *7*, 287.